

Hydrothermal Synthesis and Electrochemical Performance of Al-doped VO₂(B) as Cathode Materials for Lithium-Ion Battery

Zhengguang Zou*, Zhongliang Hou, Jilin Wang, Yao Gao, Zhendong Wan and Shichang Han

Ministry-province Jointly-constructed Cultivation Base for State Key Laboratory of Processing for Non-ferrous Metal and Featured Materials, Guilin University of Technology, Guilin, China.

*E-mail: zouzgglut@163.com

Received: 24 January 2017 / Accepted: 2 April 2017 / Published: 12 May 2017

Al-doped VO₂(B) nanobelts have been successfully synthesized via the hydrothermal method using V₂O₅, C₆H₁₂O₆·H₂O and Al(NO₃)₃·9H₂O as reactants. XRD, FESEM, EDS and XPS were introduced to characterize the phase, morphology, compositions and chemical state of the samples. Electrochemical properties of the samples were studied by charge/discharge tests, electrochemical impedance spectra (EIS) and cyclic voltammetry (CV). The result showed that the length and width of the nanobelts were increased significantly after doping Al³⁺. When the doping molar ratio of Al to V was 1/6.9, the product was flower like particles which composed of nanobelts and exhibited the best cycling performance. The initial discharge capacity was 282 mAh·g⁻¹ and maintained 202 mAh·g⁻¹ after 50 cycles at the density of 32.4 mA·g⁻¹. The retention rate of capacity was 71.6%, which was better than that of the undoped sample (61%). The enhanced electrochemical performance was attributed to its higher total conductivity and better structure stability.

Keywords: Lithium-ion battery; VO₂(B); Hydrothermal method; doping; electrochemical performance

1. INTRODUCTION

Rechargeable lithium ion batteries (LIBs) have been considered as one of the most promising candidates for the applications of electronics and electric vehicles with the potential to reduce the consumption of fossil fuels and lower the emissions of greenhouse gas [1–4]. Nevertheless, to meet the increasing demands of new generation energy storage devices such as grid-scale energy storage, portable electronic devices, and electric vehicle propulsion, high energy density rechargeable battery electrode materials with outstanding cycling stabilities and excellent rate capabilities have attracted considerable research interests worldwide [5, 6]. However, the extensive application of the lithium-ion battery was highly relied on the safety, cost, and service life, which were in turn determined by the materials used. Unfortunately, even after decades of intensive research, the commercially available

cathode materials exhibited practical capacity of less than $200 \text{ mAh}\cdot\text{g}^{-1}$, which seriously limited the further applications of LIBs [7–12]. Therefore, advanced materials with high specific capacity and excellent cycling performance are indispensable components for the next generation of LIBs.

In past decades, vanadium oxides lithium-ion batteries materials were widely researched because of their unique geometry and specific electrochemical properties. Among various potential vanadium oxides, the metastable phase $\text{VO}_2(\text{B})$ has attracted significant attention due to its layer structure, which is beneficial for Li^+ intercalation and deintercalation [13]. The monoclinic $\text{VO}_2(\text{B})$ is made up of distorted VO_6 octahedral sharing both corners and edges, forming the V-O tunnels vertical to the *c*-axis. Owing to the special structure, the maximum reversible capacity of VO_2 could reach to $320 \text{ mAh}\cdot\text{g}^{-1}$ in the range of 4–1 V in aqueous lithium battery [14–17], which is much higher than that of common cathode materials such as LiCoO_2 ($140 \text{ mAh}\cdot\text{g}^{-1}$) [18]. Based on these good characters, $\text{VO}_2(\text{B})$ has been one of the most promising cathode materials for the lithium ion batteries.

Nanostructured materials have presented special physical and chemical properties on account of their nanometer-size dimensions [19]. It was reported that nanostructured vanadium oxides could improve the electrochemical performance in contrast with their bulk counterparts [20, 21]. In recent years, various morphologies of $\text{VO}_2(\text{B})$ nanomaterials have been synthesized, including nanorods [22, 23], nanoribbons [24, 25], nanotubes [26, 27] and nanowires [28]. The nanostructured morphology significantly improved the initial discharge specific capacity of $\text{VO}_2(\text{B})$ materials [22]. In spite of these efforts, these materials were still sustained poor high-rate performance and fast capacity fading, which was probably attributed to reasons such as dissolution, self-aggregation, and the increased charge transfer resistance during the process of charging and discharging [29]. Therefore, it is eager to improve the cycling stability of $\text{VO}_2(\text{B})$.

In order to improve the electrochemical properties of $\text{VO}_2(\text{B})$, transition elements (such as Cu^{2+} and Ti^{4+}) were used as typical dopant [30]. However, their ionic radius [Cu^{2+} (0.73 Å), Ti^{4+} (0.605 Å)] were larger than V^{4+} (0.58 Å), thus they were difficult to enter into $\text{VO}_2(\text{B})$ crystal lattice and form effective doping. Conversely, aluminum is a low-cost, good conductive and environmental element in the earth crust. What is more, the radius of Al^{3+} (0.535 Å) is smaller than that of V^{4+} (0.58 Å). Based on these good qualities, element aluminum is widely applied to improve the performance of electrodes made from LiMn_2O_4 , LiCoO_2 and LiVPO_4F [31–33]. However, there are seldom reports about the effect of Al-dopant on $\text{VO}_2(\text{B})$.

Herein, Al-doped $\text{VO}_2(\text{B})$ compounds were prepared via a simple hydrothermal method. The structural, morphology, crystallinity and surface state of the samples were characterized through different testing methods. Meanwhile, a series of experiments at different doping contents were carried out to investigate the influence of Al-doping on the compositions, morphologies and electrochemical properties of $\text{VO}_2(\text{B})$ nanostructures.

2. EXPERIMENTAL

2.1. Synthesis of Al doping $\text{VO}_2(\text{B})$

All chemicals were analytical grade and used without further purification. In a typical synthesis, 0.5 g V_2O_5 and 0.4 g glucose were dissolved in 70 mL deionized water, subsequently, a

certain proportion of $\text{Al}(\text{NO}_3)_3 \cdot 9\text{H}_2\text{O}$ was added into the mixture solution. After stirring for 60 minutes at room temperature, homogeneous yellowy suspension was obtained and transferred into a 100mL teflon-lined autoclave. The autoclave was at last sealed and placed in an oven, heated to 180 °C for 24 h, and then cooled to room temperature naturally. The precipitate was centrifuged with deionized water and dried in the freeze dryer for 24 h. The molar ratios of Al to V were increased gradually from 0 to 1/5.3. The samples were designated as Al₀, Al₁, Al₂, Al₃ and Al₄, corresponding to different molar ratios of Al to V (0, 1/34.4, 1/10.3, 1/6.9 and 1/5.3).

2.2. Characterization

The morphology and structure of as-prepared products were characterized by field-emission scanning electron microscopy (FE-SEM S-4800, Hitachi) and X-ray powder diffraction (Rigaku RINT2400 with Cu K α radiation). The X-ray photoelectron spectroscopy (XPS, ESCALAB 250Xi) experiments were carried out to analyze the compositions and chemical state of the samples at room temperature. The energy-dispersive X-ray spectrometer (EDS) (Oxford company, INCA IE 350) was used to analyze the chemical composition of as-obtained samples.

2.3. Electrochemical tests

The electrochemical properties of Al-doped $\text{VO}_2(\text{B})$ nanobelts were measured using the assembled experimental cells. The working electrodes were prepared by mixing active material (70 wt %), acetylene black carbon power (20 wt %) and poly-vinylidene fluoride (PVDF) (10 wt %). Both the reference and counter electrodes were Li foils. 1 mol/L LiPF_6 in a mixture of dimethyl carbonate (DMC), ethylene carbonate (EC) and diethyl carbonate (DEC) were used as electrolyte (DMC/EC/DEC=2: 2:1 in volume). The cells were assembled in a glove box filled with pure dry argon gas. Galvanostatic charge/discharge measurements were carried out in the voltage region between 1.5 V and 4.0 V. Both the electrochemical impedance spectroscopy (EIS) and the cyclic voltammetry (CV) were tested through a CHI 760D electrochemical workstation, and the CV measurement was performed in the potential range from 3.5 to 1.5 V at a scan rate of 0.1 $\text{mV} \cdot \text{s}^{-1}$.

3. RESULTS AND DISCUSSION

3.1. Structure and morphology analysis

Figure 1(a) showed the XRD patterns of the samples with different doping content of $\text{Al}(\text{NO}_3)_3 \cdot 9\text{H}_2\text{O}$ that has been calcined at 300 °C in N_2 atmosphere for 1 h. All peaks were basically consistent with the standard diffraction peaks of $\text{VO}_2(\text{B})$ (JCPDS no. 81-2392). However, with the doping content increasing, the diffraction peaks broaden and the intensity weaken, which was attributed to the crystallinity decrease after doping with Al^{3+} . It could also be seen that the diffraction peaks were slightly shift to the higher angle direction after doping Al^{3+} (Figure 1(b)), which was

attributed to the smaller radius of Al^{3+} (0.535 Å) than that of V^{4+} (0.58 Å), indicating the successfully incorporation of Al into the $\text{VO}_2(\text{B})$ lattice.

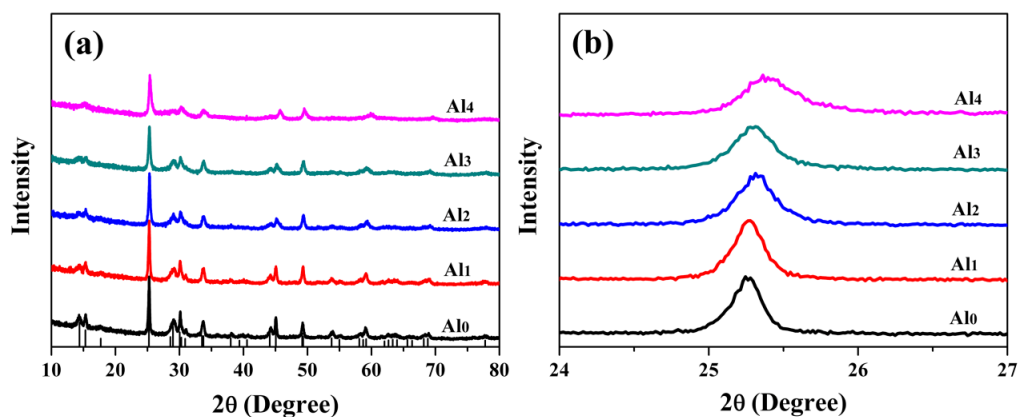


Figure 1. (a) XRD patterns of Al_0 , Al_1 , Al_2 , Al_3 , Al_4 and (b) their high angle patterns at 2θ degree ranging from 24° to 27° .

In order to investigate the composition and the valence state of the as-prepared products, XPS measurements were carried out, and the results were shown in figure 2 and figure 3. Fitted by Shirley function with software XPS peak 4.1, figure 2 showed the V 2p XPS spectra of samples with different Al^{3+} doping contents.

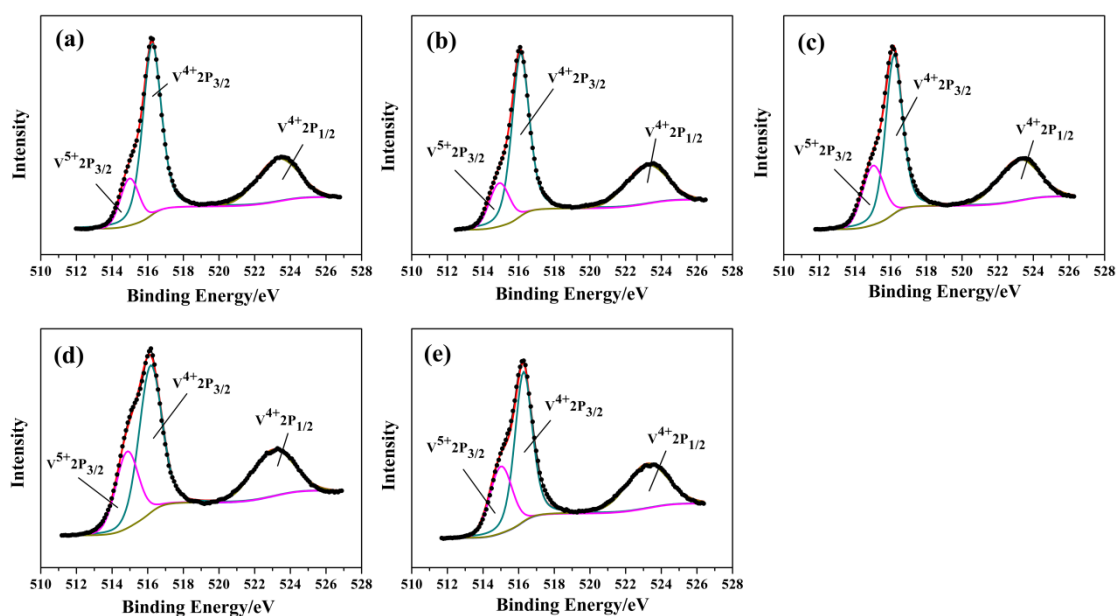


Figure 2. (a)-(e) V $2p_{3/2}$ and V $2p_{1/2}$ XPS spectra of Al_0 , Al_1 , Al_2 , Al_3 , Al_4 , respectively.

The result displayed that both +4 and +5 valence states of the vanadium element existed in all samples. The binding energy appeared at 523.29, 516.23 and 514.98 eV in the sample of Al_0 could be assigned to $\text{V}^{4+} 2p_{1/2}$, $\text{V}^{4+} 2p_{3/2}$ and $\text{V}^{5+} 2p_{3/2}$ peaks respectively [28, 34]. However, after doping Al^{3+} ,

The binding energy was slightly shifted to lower values compared to the pure one, the peak positions of $V^{4+} 2p_{1/2}$, $V^{4+} 2p_{3/2}$ and $V^{5+} 2p_{3/2}$ were originated from 523.18, 516.19 and 514.90 eV for Al₁, through 523.16, 516.18 and 514.88 eV for Al₂, 523.05, 516.15 and 514.86 eV for Al₃, to 523.19, 516.20 and 514.90 eV for Al₄. The decrease of the binding energy indicated that the incorporation of Al^{3+} has weakened the interaction between the vanadium and oxygen elements [35]. From fitted curves in Figure 2, the ratio of $V^{4+} 2p_{3/2} / V^{5+} 2p_{3/2}$ were 4.2/1, 3.8/1, 2.45/1, 2/1 and 2.05/1 for the samples of Al₀, Al₁, Al₂, Al₃ and Al₄, respectively. The result suggested that the major oxidation state of V was +4, which was consistent with that of the XRD results. The proportion increased of V^{5+} in the system may be attributed to Al^{3+} replace the site of V^{4+} . Figure 3 presented the Al 2p XPS spectra of samples with different Al^{3+} doping contents. Two peaks located at about 68.9 eV and 73.1 eV in each sample, which could be assigned to V 3s and $Al^{3+} 2p$ respectively [36–38]. Owing to the increased dopant concentration, the intensity of Al peak boosted.

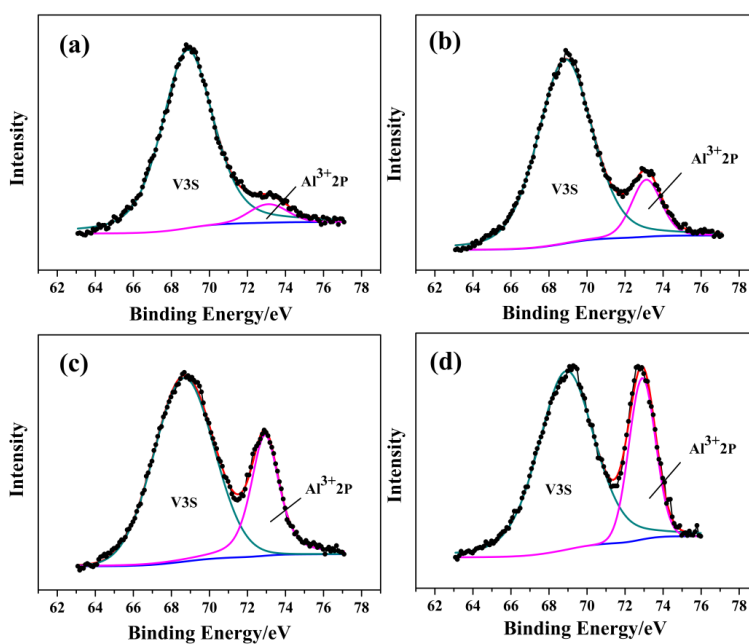


Figure 3. Al2p XPS spectra of Al₁(a), Al₂(b), Al₃(c) and Al₄(d).

The FESEM images of pure VO₂(B) and Al-doped samples were shown in figure 4. The doping content of Al^{3+} was significant effect on the morphologies of as-synthesized products. The sample without doping was consisted of belt-like particles with a length of several hundred nanometers and a width of 100-200 nm. After doping Al^{3+} , the length and width of the nanobelts were increased gradually. However, the samples of Al₁ and Al₂ exhibited more or less agglomeration, which may be attributed to the large surface. Compared with Al₁ and Al₂, the samples with high doping content (Al₃ and Al₄) were flower-like structures which composed of nanobelts. In particular, a large number of spaces emerged in the adjacent belts, which was more obvious in the sample of Al₃. This special structure was beneficial to the transport of the electron/ion between the cathode material and the

electrolyte. Based on this result, Li^+ insertion/extraction was much faster and it could enhance the performance of batteries.

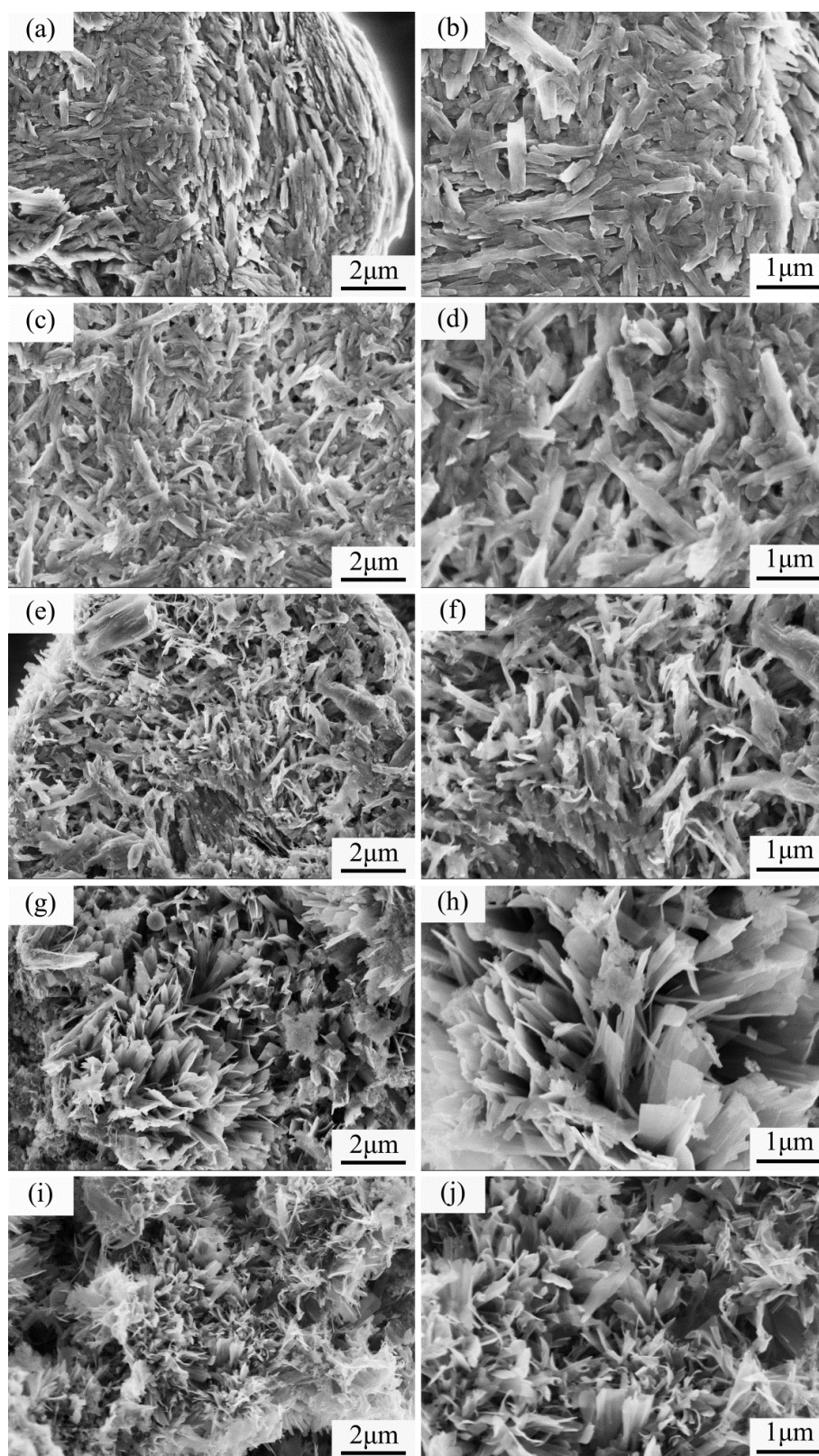


Figure 4. SEM images of Al₀(a, b), Al₁(c, d), Al₂(e, f), Al₃(g, h) and Al₄(i, j).

3.2. Energy-dispersive X-ray spectrometer (EDS)

Table 1 showed the EDS analysis of Al-doped VO₂(B) samples. All the samples composed Al, V and O, and the molar ratio of Al to V increased with the increase of doping content. However, there existed a deviation between the design and experiment, which was owing to the different precipitation rates between Al³⁺ and VO₂ in the process of synthesis [30]. The molar ratio values of Al/V measured by EDS were closed to the theoretical values, which was further demonstrated that the Al³⁺ entered into VO₂(B) lattice uniformly.

Table 1. EDS analysis of Al₀, Al₁, Al₂, Al₃ and Al₄.

The sample	The theoretical molar ratio of Al/V	The actual molar ratio of Al/V
Al ₀	0	0
Al ₁	1/34.4	1/52.1
Al ₂	1/10.3	1/14.2
Al ₃	1/6.9	1/9.0
Al ₄	1/5.3	1/8.2

3.3. Electrochemical properties

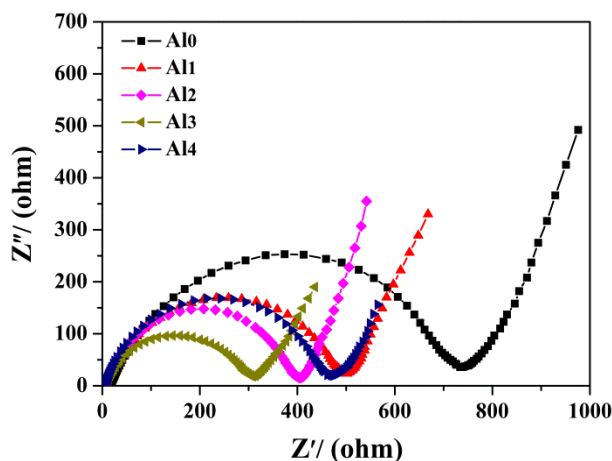


Figure 5. Nyquist plots of Al₀, Al₁, Al₂, Al₃ and Al₄.

Figure 5 showed the Nyquist plots of the samples, which were measured by electrochemical impedance spectra (EIS) with a frequency ranging from 100 kHz to 0.01 Hz after 3 cycles in the discharged state. All the plots consisted of a compressed semicircle in the high-medium frequency due to the charge transfer impedance (Rct), and a slope line in the low-frequency region, which was related to Warburg impedance (ZW) linked with the diffusion of lithium-ions in the active material. As could be seen from figure 5, the values of Rct were 795Ω (Al₀), 536.2Ω (Al₁), 436.5Ω (Al₂), 340.5Ω (Al₃) and 485.6Ω (Al₄). Obviously, The VO₂(B) electrodes exhibited smaller Rct values after doping with

Al^{3+} , in particular, the Rct value of Al_3 was found to be the lowest, which may be ascribed to appropriate doping content of Al^{3+} . The result revealed that the incorporation of Al^{3+} could improve the electronic conductivity of the samples and further result in lower electrochemical polarization and faster electron transportation, thus will lead to higher initial capacity and better cycling performance.

Table 2. The electrochemical performance of Al-doped $\text{VO}_2(\text{B})$ and the other similar cathode materials.

cathode material	current density ($\text{mAh}\cdot\text{g}^{-1}$)	initial discharge capacity ($\text{mAh}\cdot\text{g}^{-1}$)	capacity retention	cycle number
$\text{VO}_2(\text{M})$	10	81.9	7.4%	10
$\text{VO}_2(\text{B})$	10	180.33	52.8%	50
$\text{VO}_2(\text{B})$ with Multi-Wall Carbon Nanotube	50	238	63.4%	50
Al-doped $\text{VO}_2(\text{B})$ – this work	32.4	282	71.6%	50

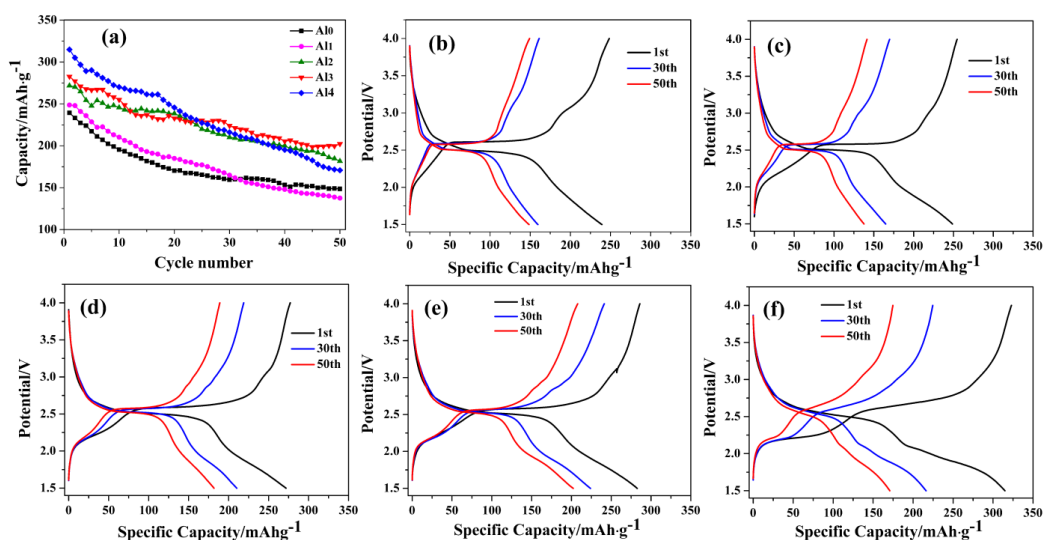


Figure 6. (a) Cycling performance of the samples at the current density of $32.4 \text{ mA}\cdot\text{g}^{-1}$, (b)-(f) discharge/charge curves of Al_0 , Al_1 , Al_2 , Al_3 and Al_4 , respectively.

Figure 6(a) displayed the cycling performance of Al-doped samples at a current density of $32.4 \text{ mA}\cdot\text{g}^{-1}$. The initial and after 50 cycles discharge capacities were $241 \text{ mAh}\cdot\text{g}^{-1}$ and $147 \text{ mAh}\cdot\text{g}^{-1}$ (Al_0), $248 \text{ mAh}\cdot\text{g}^{-1}$ and $137 \text{ mAh}\cdot\text{g}^{-1}$ (Al_1), $271 \text{ mAh}\cdot\text{g}^{-1}$ and $181 \text{ mAh}\cdot\text{g}^{-1}$ (Al_2), $282 \text{ mAh}\cdot\text{g}^{-1}$ and $202 \text{ mAh}\cdot\text{g}^{-1}$ (Al_3), $314 \text{ mAh}\cdot\text{g}^{-1}$ and $170 \text{ mAh}\cdot\text{g}^{-1}$ (Al_4). The retention rates of capacities were 61%, 55%, 67%, 71.6% and 54%, respectively. The discharge capacity of Al-doped samples had significantly improved than that of the pure one, which was attributed to better ionic and electronic conductivity of the samples after doping with Al^{3+} . It could also be seen that the capacity retention rates of the Al-doped samples has been improved greatly, among which, Al_3 showed the best cycling performance. The result suggested that doping appropriate Al^{3+} could stabilize the crystal structure of $\text{VO}_2(\text{B})$ and

reduce the irreversible destruction in cathode materials. The excellent cycling performance of Al_3 was ascribed to its special flower-like structure which permitted Li^+ insertion/extraction quickly from the materials. The result showed that the electrochemical performance of Al-doped $\text{VO}_2(\text{B})$ was significantly better than the other similar cathode materials [39, 40], as showed in Table 2.

Figure 6 (b) to (f) showed the 1st, 30th and 50th charge-discharge curves of different doping content of the samples at the current density of $32.4 \text{ mA} \cdot \text{g}^{-1}$ in the voltage ranging from 1.5 V to 4.0 V at room temperature. All of them showed a distinct discharge platform at around 2.4 V, which was attributed to the reduction of V^{5+} to V^{4+} [41, 42], the result was agreement with that of the reference [22, 23, 43]. The platform near 2.4 V in the sample of Al_4 became more inconspicuous after cycling for 50 times, indicating that more irreversible reaction existed in the process of Lithium ion insertion and extraction from the cathode material. In contrast, the sample of Al_3 still showed a more distinct charge and discharge platform after cycling for 50 times, demonstrating a better electrochemical property, which was in accordance with the cycling performance results (Figure 6(a)).

Figure 7 showed the cyclic voltammetry (CV) curves of Al_0 (a), Al_1 (b), Al_2 (c), Al_3 (d) and Al_4 (e) with the voltage range of 1.5-3.5 V at the scanning speed of 0.1 mV/s after charging/discharging 3 cycles. It could be obviously observed a pair of oxidation and reduction peaks in these samples, which represented the Li^+ extraction and insertion from the structure of monoclinic $\text{VO}_2(\text{B})$. For the sample of Al_0 , the characteristic oxidation and reduction peak centered at 2.85 V and 2.35 V, indicating the cathode materials carried out an extraction and intercalation of Li^+ . In addition, two weak oxidation peaks (2.2 V and 3.14 V) were observed, which could be assigned to the oxidation process of low-valent vanadium oxides with low content [44].

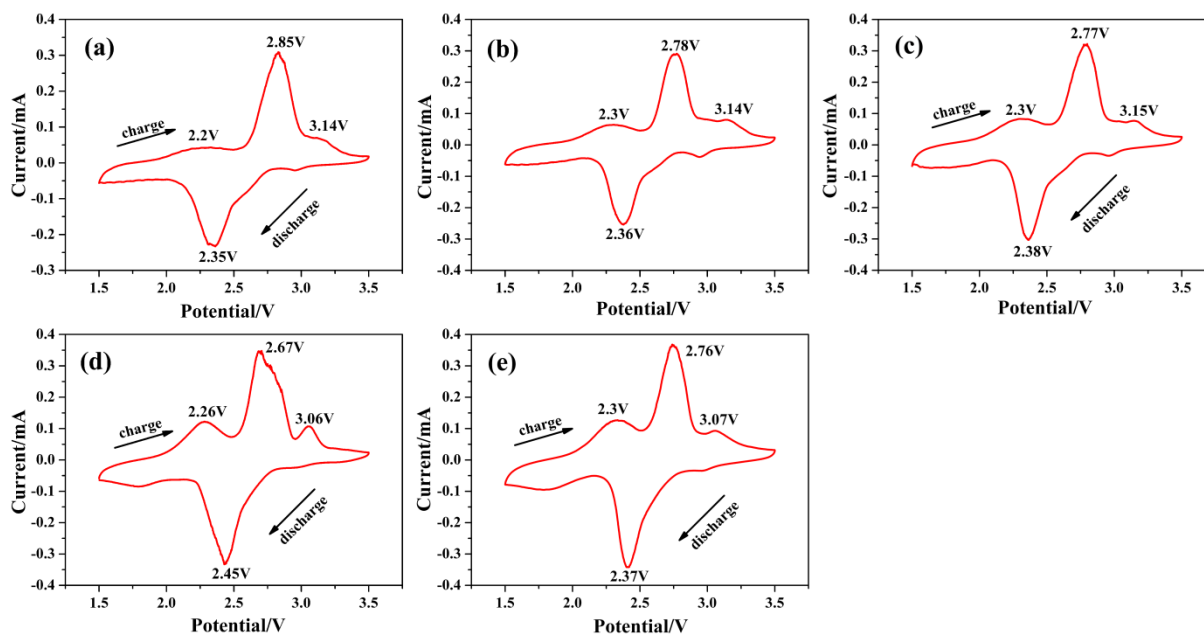


Figure 7. Cyclic voltammetry (CV) curves of Al_0 (a), Al_1 (b), Al_2 (c), Al_3 (d) and Al_4 (e).

The main redox peak potentials were in accordance with the literature [45]. With the doping content increasing, the reduction peaks shifted to higher voltage and the oxidation peaks shifted to

lower voltage, indicating that the incorporation of Al^{3+} could affect the mobility of lithium ion. The highest symmetry of the oxidation peaks and reduction peaks of Al_3 presented the best cycling performance of all the samples, which were consistent with the cycling performance test results mentioned-above.

4. CONCLUSION

In conclusion, Al-doped $\text{VO}_2(\text{B})$ nanobelts were synthesized via a simple hydrothermal method with V_2O_5 , $\text{C}_6\text{H}_{12}\text{O}_6 \cdot \text{H}_2\text{O}$ and $\text{Al}(\text{NO}_3)_3 \cdot 9\text{H}_2\text{O}$ as reactants. It was found that the incorporation of Al^{3+} significantly effect on the morphology and structure of $\text{VO}_2(\text{B})$. With the doping content increasing, the length and width of the nanobelts were increased gradually, meanwhile, The flower-like structures composed of nanobelts were obtained when the molar ratio of Al to V increased to 1/6.9. Electrochemical properties demonstrated that the charge/discharge capacity and the cyclic stability of the samples have been improved greatly after doping with Al^{3+} . In particular, the sample of Al_3 exhibited best electrochemical performance, The initial discharge capacity was $282 \text{ mAh} \cdot \text{g}^{-1}$ and maintained $202 \text{ mAh} \cdot \text{g}^{-1}$ after 50 cycles at the density of $32.4 \text{ mA} \cdot \text{g}^{-1}$. The retention rate of capacity was 71.6%. The enhanced electrochemical performance was attributed to its higher total conductivity and better structure stability. The good performances of these materials indicated their potential application in lithium-ion batteries. We hope that this work can provide reference for the lithium-ion battery research and its application.

ACKNOWLEDGEMENTS

The authors gratefully acknowledge the National Nature Science Foundation of China (project no. 51562006)

References

1. J. M. Tarascon and M. Armand, *Nature*, 414 (2001) 359.
2. C. Z. Yuan, H. B. Wu, Y. Xie and X. W. Lou, *Angew. Chem. Int. Edit.*, 53 (2014) 1488.
3. R. V. Noorden, *Nature*, 507 (2014) 26.
4. J. Jiang, Y. Y. Li, J. P. Liu, X. T. Huang, C. Z. Yuan and X. W. Lou, *Adv. Mater.*, 24 (2012) 5166.
5. T. H. Kim, J. S. Park, S. K. Chang, S. D. Choi, J. H. Ryu and H. K. Song, *Adv. Energy Mater.*, 2 (2012) 860.
6. N. S. Choi, Z. H. Chen, S. A. Freunberger, X. L. Ji, Y. K. Sun, K. Amine, G. Yushin, L. F. Nazar, J. Cho and P. G. Bruce, *Angew. Chem. Int. Edit.*, 5 (2012) 19994.
7. J. W. Fergus, *J. Power Sources*, 195 (2010) 939.
8. M. K. Song, S. J. Park, F. Alamgir, J. P. Cho and M. Liu *Mat. Sci. Eng. R*, 72 (2011) 203.
9. K. T. Lee and J. Cho, *Nano Today*, 6 (2011) 28.
10. J. B. Goodenough and Y. Kim, *Chem. Mater.*, 22 (2010) 587.
11. B. Kang and G. Ceder, *Nature*, 458 (2009) 190.
12. M. Armand and J. M. Tarascon, *Nature*, 451 (2008) 652.
13. T. Chirayil, P. Y. Zavalij and M. S. Whittingham, *Chem. Mater.*, 10 (1998) 2629.
14. D. W. Murphy and P. A. Christian, *Science*, 205 (1979) 651.
15. J. Glanz, *Science*, 264 (1994) 1084.

16. N. A. Chernova, M. Roppolo, A. C. Dillon and M. S. Whittingham, *J. Mater. Chem.*, 19 (2009) 2526.
17. E. Baudrin, G. Sudant, D. Larcher, B. Dunn and J. M. Tarascon, *Chem. Mater.*, 18 (2006) 4369.
18. K. S. Kang, Y. S. Meng, J. Breger, C. P. Grey and G. Ceder, *Science*, 311 (2006) 977.
19. A. P. Alivisatos, *Science*, 271 (1996) 933.
20. N. Ding, X. Y. Feng, S. H. Liu, J. Xu, X. Fang, I. Lieberwirth and C. H. Chen, *Electrochem. Commun.*, 11 (2009) 538.
21. K. H. Seng, J. Liu, Z. P. Guo, Z. X. Chen, D. Z. Jia and H. K. Liu, *Electrochem. Commun.*, 13 (2011) 383.
22. Z. J. Chen, S. K. Gao, L. L. Jiang, M. D. Wei and K. M. Wei, *Mater. Chem. Phys.*, 121 (2010) 254.
23. C. V. S. Reddy, E. H. Walker, S. A. Wicker, Q. L. Williams and R. R. Kalluru, *Curr. Appl. Phys.*, 9 (2009) 1195.
24. L. J. Mao and C. Y. Liu, *Mater. Res. Bull.*, 43 (2008) 1384.
25. G. C. Li, S. P. Pang, L. Jiang, Z. Y. Guo and Z. K. Zhang, *J. Phys. Chem. B*, 110 (2006) 9383.
26. M. Niederberger, H. J. Muhr, F. Krumeich, F. Bieri, D. Gunther and R. Nesper, *Chem. Mater.*, 12 (2000) 1995.
27. F. Krumeich, H. J. Muhr, M. Niederberger, F. Bieri, B. Schnyder and R. Nesper, *J. Am. Chem. Soc.*, 121 (1999) 8324.
28. X. Y. Chen, X. Wang, Z. H. Wang and Y. T. Qian, *Nanotechnology*, 15 (2004) 1685.
29. H. M. Liu, Y. G. Wang, K. X. Wang, E. Hosono and H. S. Zhou, *J. Mater. Chem.*, 19 (2009) 2835.
30. H. Cheng, *Fabrication, doping and the electrochemical properties of vanadium oxide*, Dissertation, China, Guilin University of Technology (2014).
31. D. Zhan, Y. Liang, P. Cui and Z. A. Xiao, *RCS Adv.*, 5 (2015) 6372.
32. H. T. Xu, H. J. Zhang, L. Liu, Y. Y. Feng and Y. Wang, *ACS Appl. Mater. Inter.*, 7 (2015) 20979.
33. X. J. Lv, Z. M. Xu, L. Jie, J. G. Chen and Q. S. Liu, *J. Solid State Chem.*, 239 (2016) 228.
34. X. H. Liu, G. Y. Xie, C. Huang, Q. Xu, Y. F. Zhang and Y. B. Luo, *Mater. Lett.*, 62 (2008) 1878.
35. X. F. Wu, Z. M. Wu, C. H. Ji, H. F. Zhang, Y. J. Su, Z. H. Huang, J. Gou, X. B. Wei, J. Wang and Y. D. Jiang, *ACS Appl. Mater. Inte.*, 8 (2016) 11842.
36. M. Chen, X. Wang, Y. H. Yu, Z. L. Pei, X. D. Bai, C. Sun, R. F. Huang and L. S. Wen, *Appl. Surf. Sci.*, 158 (2000) 134.
37. J. P. Kar, S. Kim, B. Shin, K. I. Park, K. J. Ahn, W. Lee, J. H. Cho and J. M. Myoung, *Solid State Electro.*, 54 (2010) 1447.
38. K. Uma, M. Rusop, T. Soga and T. Jimbo, *Jpn. J. Appl. Phys.*, 46 (2007) 40.
39. J. Ni, W. T. Jiang, K. Yu, F. Sun and Z. Q. Zhu, *Cryst. Res. Technol.*, 46 (2011) 507.
40. X. W. Zhou, G. M. Wu, G. H. Gao, C. J. Cui, H. Y. Yang, J. Shen, B. Zhou and Z. H. Zhang, *Electrochim. Acta*, 74 (2012) 32.
41. Y. Piffard, F. Leroux, D. Guyomard, J. L. Mansot and M. Tournoux, *J. Power Sources*, 68 (1997) 698.
42. F. Hu, C. H. Zhang, S. Zhang, X. Ming, G. Chen, Y. J. Wei and C. Z. Wang, *Chem. Res. In Chinese U.*, 27 (2011) 528.
43. F. Sediri, F. Touati and N. Gharbi, *Mat. Sci. Eng. B-Solid*, 129 (2006) 251.
44. Q. Q. Zhao, L. F. Jiao, W. X. Peng, H. Y. Gao, J. Q. Yang, Q. H. Wang, H. M. Du, L. Li, Z. Qi, Y. C. Si, Y. J. Wang and H. T. Yuan, *J. Power Sources*, 199 (2012) 350.
45. M. M. Rahman, J. Z. Wang, N. H. Idris, Z. X. Chen and H. K. Liu, *Electrochim. Acta*, 56 (2010) 693.